Observation-based solar and wind power capacity factors and power densities

Environmental Research Letters

LETTER

Observation-based solar and wind power capacity factors and power densities

Lee M Miller[1,3] and David W Keith[1,2]

[1] School of Engineering and Applied Sciences, Harvard University, Cambridge, MA 02139, United States of America
[2] Harvard Kennedy School, Cambridge, MA 02138, United States of America
[3] Author to whom any correspondence should be addressed.

E-mail: lmiller@seas.harvard.edu **and** david_keith@harvard.edu

Keywords: power density, capacity factor, renewable energy, land use, photovoltaics, solar power, wind power

Supplementary material for this article is available online

OPEN ACCESS

RECEIVED
22 June 2018

REVISED
7 September 2018

ACCEPTED FOR PUBLICATION
13 September 2018

PUBLISHED
4 October 2018

Abstract

Power density is the rate of energy generation per unit of land surface area occupied by an energy system. The power density of low-carbon energy sources will play an important role in mediating the environmental consequences of energy system decarbonization as the world transitions away from high power-density fossil fuels. All else equal, lower power densities mean larger land and environmental footprints. The power density of solar and wind power remain surprisingly uncertain: estimates of *realizable* generation rates per unit area for wind and solar power span 0.3–47 $W_e\ m^{-2}$ and 10–120 $W_e\ m^{-2}$ respectively. We refine this range using US data from 1990–2016. We estimate wind power density from primary data, and solar power density from primary plant-level data and prior datasets on capacity density. The mean power density of 411 onshore wind power plants in 2016 was 0.50 $W_e\ m^{-2}$. Wind plants with the largest areas have the lowest power densities. Wind power capacity factors are increasing, but that increase is associated with a decrease in capacity densities, so power densities are stable or declining. If wind power expands away from the best locations and the areas of wind power plants keep increasing, it seems likely that wind's power density will decrease as total wind generation increases. The mean 2016 power density of 1150 solar power plants was 5.4 $W_e\ m^{-2}$. Solar capacity factors and (likely) power densities are increasing with time driven, in part, by improved panel efficiencies. Wind power has a 10-fold lower power density than solar, but wind power installations directly occupy much less of the land within their boundaries. The environmental and social consequences of these divergent land occupancy patterns need further study.

Introduction

Wind and solar power generation have grown dramatically, yet they still generate only a small fraction of electricity or of primary energy. In 2017, for example, wind and solar generated 6.0% and 1.8% respectively of US electricity (BP 2018). Wind and solar, like all energy systems, occupy land, displacing natural systems, agriculture, and human communities. Power density, the energy generation rate per time per unit ground area (expressed here as $W_e\ m^{-2}$), is one important measure of the land use of energy systems (Smil 1984, 2015, MacKay 2009, 2013a, 2013b). Use of low-carbon energy sources such as wind and solar may increase dramatically as the energy systems is decarbonized to limit climate risks. Quantitative estimates of power densities are therefore important in understanding the scope and impacts of low-carbon energy systems. Yet, as we describe below, existing power density estimates for wind and solar are inconsistent. Here we estimate the power density of wind and solar power using data that includes most grid-connected commercial-scale installations in the US. We also examine how power densities vary with power plant age and size.

For wind power, estimates of the power density vary by about a factor of 70. Technological innovations in turbine design and arrangement show that up to 47 $W_e\ m^{-2}$ is achievable over very small areas

(Dabiri 2011). For onshore wind power plants at county- to country-scales, estimates fall in the range of 3.5–7.0 $W_e\,m^{-2}$ assuming one wind turbine does not affect the generation of downwind turbines (Archer and Jacobson 2005, Lu *et al* 2009, Sta. Maria and Jacobson 2009, Jacobson and Delucchi 2011). Smaller estimates of 0.5–1.0 $W_e\,m^{-2}$ emerge from analysis that considers turbine–atmosphere interactions (Gustavson 1979, Keith *et al* 2004, Wang and Prinn 2010, Miller *et al* 2011, 2015, Gans *et al* 2012, Jacobson and Archer 2012, Marvel *et al* 2012, Adams and Keith 2013, Miller and Kleidon 2016).

Note that all the values in the preceding paragraph, and throughout this paper, refer to the average annual power density over the entire areal extent of the wind farm, hereafter 'wind power plant'. This power density of wind power plants is much smaller than the power density computed by counting only the area directly occupied by infrastructure, such as the turbine pads and access roads (MacKay 2013a, Smil 2015). Including the whole area of the wind power plant when calculating wind power density is critical to establishing the reproducibility of similar plants in adjacent locations, which informs wind power's generation potential at larger scales. The land use considerations of wind power are complex. While the open space betwen turbines is critical to minimizing turbine–turbine and turbine–atmosphere interactions, that same open space is usually co-utilized for other purposes like agriculture. Note that we defer to the Methods section the real-but-tractable issues of quantifying that area given knowledge of the wind turbine locations.

For solar photovoltaics (PV), estimates of the power density differ by about a factor of 12. The low-end estimates by MacKay and Smil are the 3–9 $W_e\,m^{-2}$ (MacKay 2013b, Smil 2015). Kammen and Sunter (2016) estimate that typical values are 10 $W_e\,m^{-2}$, while Hernandez *et al* (2015) suggest values of 47–66 $W_e\,m^{-2}$ for sunny regions like California, and Kammen and Sunter (2016) estimate a technical potential of 120 $W_e\,m^{-2}$ if such sunny flat regions were blanketed with today's highest (~40%) efficiency PV panels. Underlying these estimates are different assumptions regarding panel efficiency, the ratio of fraction of the land surface area to PV panels area, and whether the angle of the panels is fixed or uses 1- or 2-axis solar tracking.

Here we estimate the power densities and capacity factors for wind and solar power plants with AC-capacities greater than 1 MW which generated electricity in the US during 1998–2016. For wind we make a direct plant-by-plant bottom-up estimate while for solar our estimates of power density depend on a correlation analysis that provides a single estimate for the solar installed capacity density.

Data sources and methods

We used four data sources:

- EIA Power Plants, hereafter *Power Plants*, published on 19 April 2018 and current through January 2018 (US Energy Information Administration EIA 2018a). This base dataset provides status (operating, on standby, or short- or long-term out of service), a 3- to 5-digit unique 'Plant Code', geographic location, name, and nameplate AC-capacity for 1043 wind power plants and 2227 solar PV power plants.
- EIA Bulk Data, hereafter *Electricity Generation* (US Energy Information Administration EIA, 2018b). This data set includes monthly electricity generation data for each power plant through December 2016 including geographic location, name, and a 'series id' that is the same as the Plant Code in *Power Plants*. Note that most data is missing for power plants first operational in 2016.
- EIA-860, hereafter *Detailed Data,* published April 2018 (US Energy Information Administration EIA 2018c). This data set provides AC- and DC-capacity of the power plant, month and year of first operation, referenced by Plant Code.
- United States Wind Turbine Database, hereafter *USWTDB,* published April 2018 (current through early 2018) (Hoen *et al* 2018). This data set provides locations of 57 636 wind turbines, name of the wind power plant, number of turbines in the wind power plant, turbine nameplate capacity, and rotor diameter. It does not provide a Plant Code.

Following our Wind and Solar Methods (below), we computed annual averages from monthly generation (MWh/month) when 7 or more months of data is reported rather than using the data's annual averages (MWh yr^{-1}) which would obscure pre-startup or offline periods. Only about half of all wind and solar power plants were used in our analysis for the year 2016, with this ratio varying by technology and year. These solar and wind power plants were excluded because: (a) *Power Plants* could not be linked to *Electricity Generation* based on Plant Code, or (b) capacity factors calculated from the *Power Plants* and *Electricity Generation* exceeded 100%, or (c) *Electricity Generation* was zero or unreported for more than 6 months in a given year, (d) AC-capacities between *Power Plants* and *Detailed Data* differed by more than ±10%, or finally in the case of wind power, (e) if the resulting installed capacity density was less estimated to be less than 0.1 $MW_i\,km^{-2}$.

These exclusions and filtering result in discrepancies between our dataset and those of the US Energy Information Administration EIA (2018d). For 2016, the cumulative capacity of the wind power plants included in our data was 58% the EIA's estimate for total wind capacity while for solar capacity that figure was 53% (US Energy Information Administration EIA 2018d). Our base *Power Plants* data collated power plants through early 2018, but does not specify

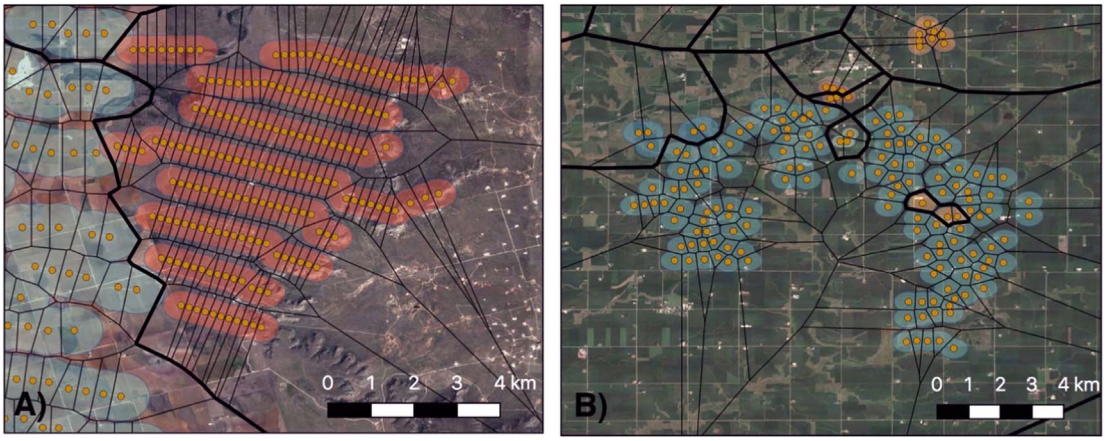

Figure 1. Illustrating Voroni-polygon and buffer-based approaches for estimating the area of wind power plants. Individual turbine locations shown as orange dots, with the thin black line around each wind turbine designating the Voroni polygon boundary. The thick black lines designate Voroni polygons surrounding each wind power plant. The colored buffer regions illustrate an alternative approach for estimating are, shown as an 8-rotor diameter (8D) buffer around each turbine. (A) Bull Creek (orange, top left, −101.6°E, 32.9°N) has an area of 243 km^2 according to (Denholm *et al* 2009), 47.8 km^2 using the 8D buffer, and 54 km^2 based on the median Voroni polygon area (0.3 km^2 per turbine with 180 turbines). (B) Fenton Wind Farm (teal, −93.2°E, 42.6°N) has an area of 156 km^2 according to (Denholm *et al* 2009), 100 km^2 using the 8D buffer, and 137 km^2 based on the median Voroni polygon area (1.0 km^2 per turbine with 137 turbines).

when the power plant came online, preventing capacity for 2016 from being quantified. *Detailed Data* provides nameplate capacity and month-year per power plant, but for 2016, total capacities are 109% and 150% the capacity for wind and solar respectively compared to (US Energy Information Administration EIA 2018d). To verify that no region was systematically excluded, we spatially compared the raw EIA *Power Plant* locations (US Energy Information Administration EIA 2018a) to those making it through our methodology, and found no obvious spatial gaps.

Wind methods

Our approach for quantifying the area of US wind power plants begins with the location of the 57 636 wind turbines in the *USWTDB* (Hoen *et al* 2018). Voroni polygons were calculated for each wind turbine using QGIS Development Team (2018). Using spatial linking, the Voroni polygons were linked to the *Power Plants* (US Energy Information Administration EIA 2018a) and then filtered for an equivalent AC-installed capacity. The Plant Code in the *Power Plants* data was then used as the unique identifier for linking to *Electricity Generation* (US Energy Information Administration EIA 2018a, 2018b) and *Detailed Data* (US Energy Information Administration EIA 2018c). Capacity factors (MW_e/MW_i) of wind power plants are calculated from *Electricity Generation* and *Power Plants* (US Energy Information Administration EIA 2018a, 2018c). Spatial and temporal curtailment by the grid operator was not included in this analysis, but will influence the results slightly (e.g. ERCOT region of Texas in 2009).

There is no well-established method to compute the area of each wind power plant. To do so, we compute a Voroni polygon (after Гео́ргий Воронóй) using QGIS Development Team (2018) for each wind turbine in the *USWTDB* which delineates the ground area that is closest to each individual turbine location compared to every other turbine. The Voroni polygon areas for wind turbines on the edge of wind power plants are very large, but the interior Voroni polygons are a useful quantification of the ground surface area per turbine. We compute the median Voroni polygon area for each wind power plant and then estimate the area of the wind power plant by multiplying this median Voroni polygon area by the number of wind turbines listed in the USWTDB (Hoen *et al* 2018).

These steps yield the wind power plant area (km^2), power density ($W_e\,m^{-2}$), installed capacity density ($MW_i\,km^{-2}$), and capacity factor for 411 wind power plants operating in 2016 (43.7 GW_i).

The advantage of this approach is that it only depends on the turbine locations and is independent from any rules-of-thumb, such as the typical spacing of 6-to-8 rotor diameters, or proprietary turbine information used by the developer as part of the wind power plant's design. This approach is also responsive to differences in arrangement (parallel rows, ridgetop or coastal alignment) and between-turbine spacing due to taller hub-heights or larger rotor diameters, without prescribing any details other than the geographic location.

To illustrate how our approach performs, we selected 2 dissimilar wind power plants from a prior study of wind power plant area (Denholm *et al* 2009) that are still in operation as of 2016. At Bull Creek (figure 1(A)), the smaller Voroni polygon areas at the interior of the wind farm contrast with those larger areas of the edge turbines but are not a problem—wind farm area is estimated from the median Voroni polygon area and the turbine count. An 8 rotor

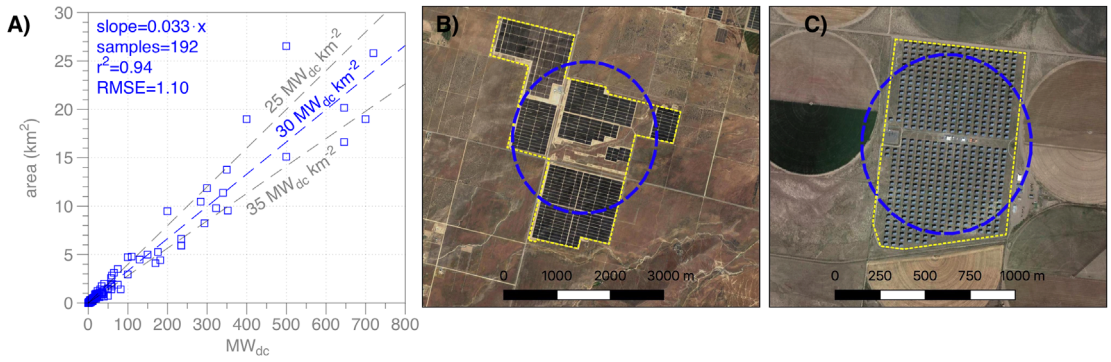

Figure 2. Relationship between rated capacity and total area of solar PV power plants. (A) Scatter plot using data of (Ong *et al* 2013) showing the linear best-fit line and statistics in blue, with the gray lines illustrating the range of the data. The two subplots to the right compare predicted and measured areas for solar power plants with very different panel efficiencies. (B) AV Solar Ranch One in California: 11% efficiency panels and 1-axis tracking installed over a large area: yellow area is 11.2 km^2, blue area using the best-fit of (A) is 9.7 km^2, and the area measured by (Ong *et al* 2013) was 10.5 km^2, C) Cogentrix in Colorado, which uses relatively high 31% efficiency panels and 2-axis tracking over a smaller area: yellow area is 1.4 km^2, blue area using the best-fit of (A) is 1.3 km^2, and the area measured by (Ong *et al* 2013) was 1.1 km^2.

diameter buffer is shown for comparison, and with its open space between rows, would underestimate the total wind farm area. The spatial overlap of these buffer regions with the wind turbine buffers to the west is also shown, with the Voroni polygons responsive to these adjacent wind farms and adjusted accordingly (see figure S1 for 4 examples, available online at stacks.iop.org/ERL/13/104008/mmedia). Fenton Wind Farm is shown in figure 1(B). This wind power plant occupies a larger area than Bull Creek, with its C-shaped turbine arrangement and spatial mixing with other wind farms showing the decisions required to estimate wind farm area, as well as the benefits of using our spatially consistent approach which can be updated as more wind turbines are deployed.

Solar methods

Our solar dataset begins with *Power Plants* (US Energy Information Administration EIA 2018a). Using the unique Plant Code, we linked this file to *Electricity Generation* (US Energy Information Administration EIA 2018b), resulting in 1311 solar PV power plants. To reduce errors, we compare the installed capacity (MW_{ac}) values with the same Plant Code between *Power Plants* and *Detailed Data* (US Energy Information Administration EIA 2018a), excluding the solar power plants that differ by ±10%, leaving 1150 solar power plants for our 2016 analysis (7.9 GW_{ac}, 9.8 GW_{dc}).

Unlike the wind methodology, we do not estimate the area of individual solar power plants from a primary dataset. Instead, we estimate the area of each solar PV farm by dividing its DC capacity from the *Detailed Data* by a fixed capacity density value of 30 $MW_{dc}\,km^{-2}$.

This capacity density value is derived from a study that assessed the area and DC capacity for 192 solar PV power plants in the US (Ong *et al* 2013). For area, we use Ong *et al*'s *total area*, which is based on environmental impact statements, project applications, and satellite imagery, and describes the area enclosing the solar arrays, roads, substations, and service buildings. A linear fit to the (Ong *et al* 2013) data yields a best-fit at 30.05 $MW_{dc}\,km^{-2}$ (figure 2). This agrees well with the installed capacity density of 25–35 $MW_{dc}\,km^{-2}$ observed in California (Hernandez *et al* 2014).

One might expect that higher panel efficiencies or tracking would produce higher generation rates per unit area. We tested this assumption by binning the (Ong *et al* 2013) data that included PV panel efficiency (109 of 192 total data points) into two sets. The first with efficiencies greater than the median (14%) and the second with efficiencies less than the median (figure S2), and then separately estimating the best-fit capacity density for the two sets. The two results differ by only 1.2% suggesting that capacity density varies little with module efficiency.

Power density (i.e. areal power generation rate, $W_e\,m^{-2}$) was calculated as:

$$PD = CD_{ac}/(CD_{dc}/(30\ MW_{dc}\,km^{-2})),$$

where CD_{ac} and CD_{dc} are the capacity densities measured on an AC or DC basis, and PD is the power density. Capacity factor was calculated from *Electricity Generation* (US Energy Information Administration EIA 2018b) and installed maximum AC capacity (MW_{ac}) from *Power Plants* (US Energy Information Administration EIA 2018a).

Results

Distributions of power densities and capacity factors are shown in figure 3. Considering capacity-weighted data for all power plants operational during 2016, the summary results are as follows. The mean and 90-percentile power densities for wind are 0.50 and 0.80 $W_e\,m^{-2}$, while the corresponding values for solar are 5.4 and 7.1 $W_e\,m^{-2}$. Note that systematic uncertainty in the distribution of power densities are significantly larger for solar than for wind because the

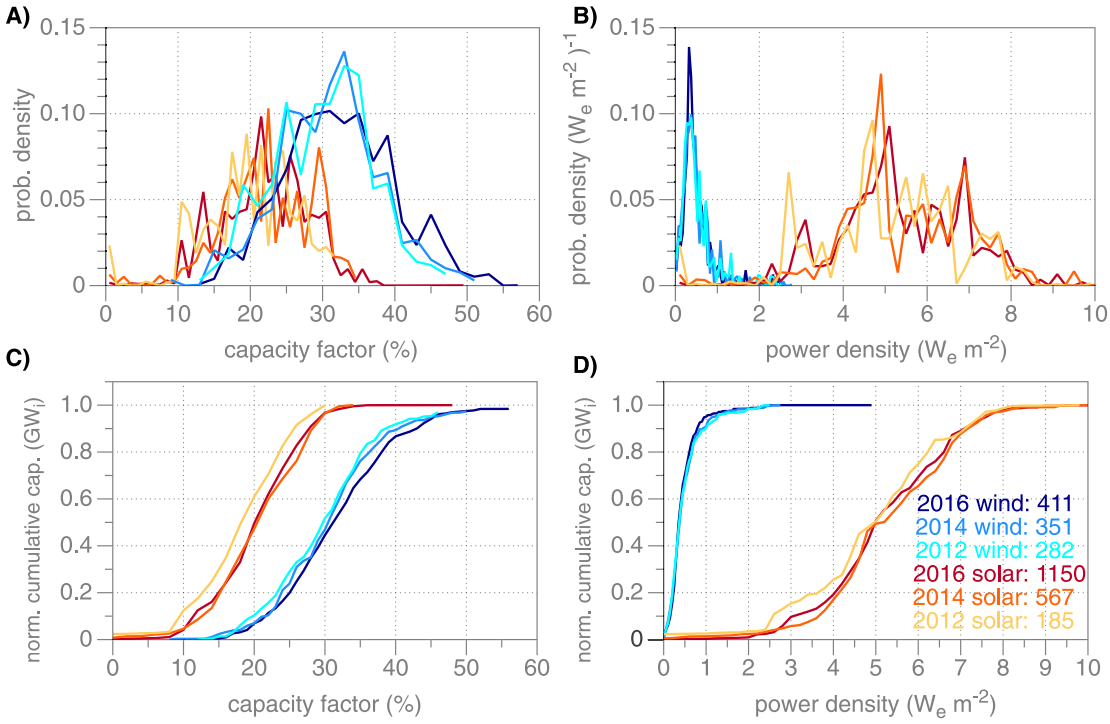

Figure 3. Distributions of capacity factors and power densities. Probability density functions (A), (B) over all wind and solar power plants; and, cumulative distribution functions of the normalized aggregated capacity (C), (D). In each case, annual average data for 2016, 2014, and 2012 is plotted, with the colored key in (D) clarifying wind from solar and the specific year.

Table 1. Solar and wind power values for the various years, with average capacity factor and average power density weighted by the installed capacity.

	Solar power				Wind power		
	Installed capacity						
Year	MW_{dc}	MW_{ac}	Capacity factor (%)	Power density (We m^{-2})	Installed capacity MW_i	Capacity factor (%)	Power density (W_e m^{-2})
2010	133	116	21.82	5.73	18 665	30.02	0.52
2011	306	267	19.08	5.00	22 693	31.37	0.52
2012	1257	1052	20.00	5.08	26 506	31.29	0.51
2013	2467	2041	22.16	5.53	33 026	30.58	0.49
2014	3876	3154	22.26	5.47	34 019	31.96	0.50
2015	5729	4660	22.09	5.41	38 262	30.77	0.46
2016	9812	7922	22.07	5.38	43 737	33.00	0.50

solar power results are derived from a fixed estimate of capacity density, whereas the wind results are computed directly. Our mean and 90-percentile capacity factors are 32.9% and 43% for wind, while the corresponding values for solar are 22.1% and 27.5%. Note that the capacity factors from EIA for 2016 are 34.5% for wind and 25.1% for solar (US Energy Information Administration EIA 2018d), and we expect that the discrepancy arises from the data sampling issues discussed above. Solar and wind power installed capacities, power densities, and capacity factors from 2010 to 2016 are shown in table 1.

Time trends are computed by binning power plants by their first year of operation (US Energy Information Administration EIA 2018b, 2018c). For solar, capacity-weighted mean capacity factors have increased by 1% per year over the years 2009–2015 (figure 4(A)). There is no significant trend in our estimate of the power density of solar power plants, but it is possible that this is an artifact of our use of a fixed DC capacity density.

Capacity factors for wind power have increased by 0.7% per year over the years 1998–2015 (figure 4(B)). The increase in wind's capacity factor is particularly evident this decade. Wind farms operating since 2010 have a mean capacity factor of 34.4% for 2010–2016, whereas the capacity factor from 1998 to 2009 is 30.9%.

There is no significant trend in the power density of wind power plants. This result is surprising given the increase in capacity factor. What underlies it? Wind power plants have three defining characteristics: the rated capacity of individual turbines, the installed capacity density of the wind farm, and the area of the wind farm. The capacity factor and power density of

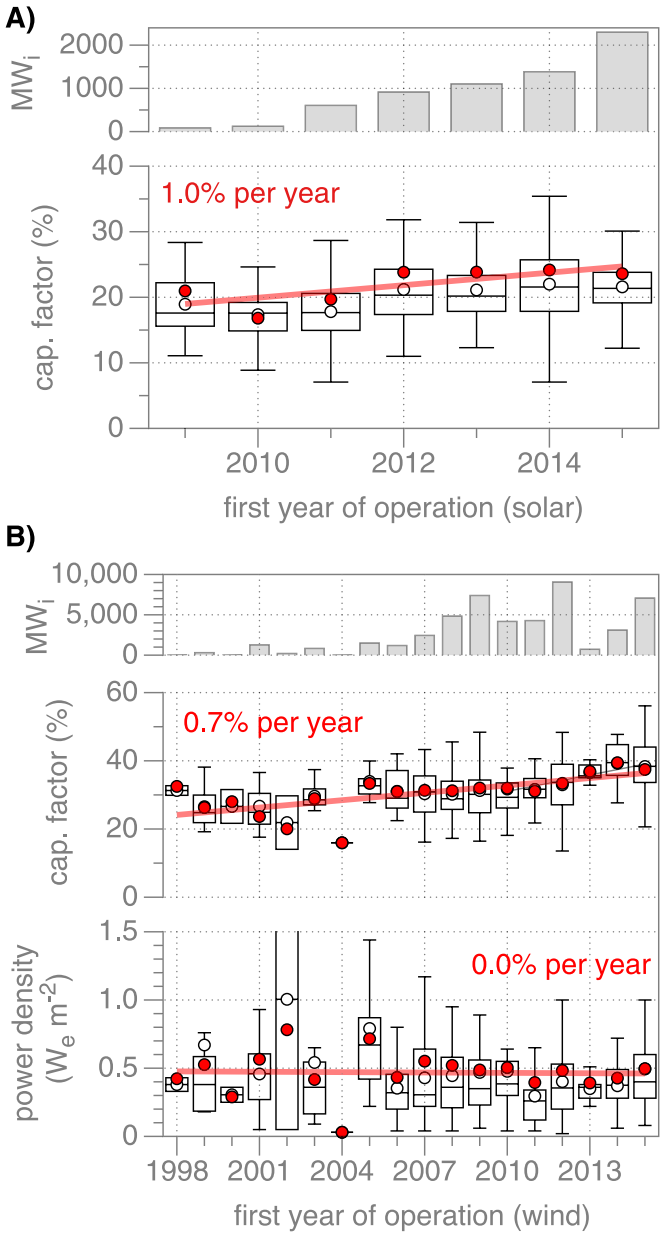

Figure 4. Age of the power plants compared to their capacity factors, and for wind their power densities. The top bars of (A), (B) show the total capacity of solar or wind power plants for that first year of operation. This first year is also used for binning the capacity factors (A), (B), and power density (B), illustrating how 2016 electricity values were influenced by the power plant's age. Box-whisker plots show the interquartile (IQR) range, white points show the means, red points show the means weighted by the individual power plant's installed capacities for that year, and the red line shows a linear fit through these weighted means. Linear fit slopes are noted in red.

the wind power plants show no relationship to the rated capacity of the individual wind turbines (figure 5(A)), whereas capacity factor and power density do vary with capacity density (figure 5(B)). Note that the highest power densities are achieved with the highest capacity densities, but the highest capacity factors are achieved with the lowest capacity densities. Treating all wind turbines and their associated Voroni polygon areas individually, a decrease in capacity density over time is apparent (figure 5(C)). The capacity density peaked at about 2.5 $MW_i\,km^{-2}$ for turbines installed between 2002 and 2005, and has since decreased to about 1.5 $MW_i\,km^{-2}$ (figure 5(D)). In summary, we find that while improved wind turbine design and siting have increased capacity factors (and greatly reduced costs) they have not altered power densities.

Figure 6 provides a map of the power densities and capacity factors for 2016. Solar capacity factors are lower on the East Coast and around the Great Lakes, and highest in the southwest where most solar power plants with capacity factors greater than 30% are located. Wind's highest capacity factors and power densities are in the Great Plains.

Finally, we examined the relationship between power plant area and power density. For solar, there is no clear relationship between area and power density (figure 7(A)), whereas for wind, there is a strong

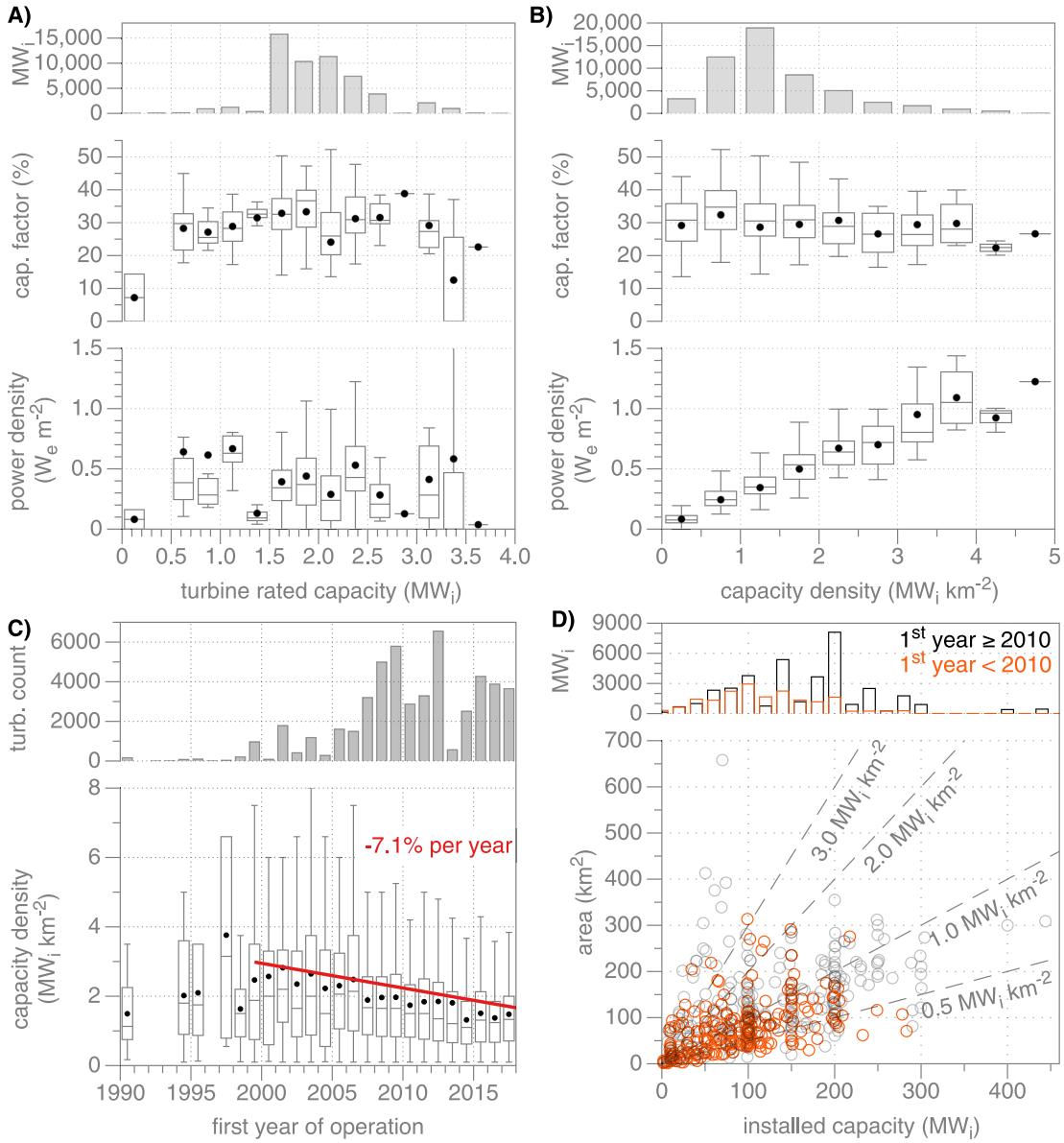

Figure 5. Design characteristics of wind power plants, and their influence on 2016 electricity generation: (A) rated capacity of the wind turbines, (B) capacity density of the wind power plant. The capacity density of 50 908 individual wind turbines is shown in (C), binned by their first year of operation, with a linear fit weighted by turbine count shown in red. In (A)–(C) all box-whisker plots show the interquartile range (IQR), with black dots indicating capacity-weighted mean values. The installed capacity of the wind power plant compared to its area is shown in (D), and uses color to discriminate between wind power plants operational before or after 2010.

relationship (figure 7(B)). While many wind power plants with areas less than 15 km^2 generate more than 1.0 $W_e\ m^{-2}$, power density decreases with increasing power plant size. This result was previously observed for 0–20 km^2 wind power plants by (MacKay 2013a). We verify this early result, and extend it by showing that wind's power density reaches an asymptote of about 0.25 $W_e\ m^{-2}$ when the wind farm area exceeds about 150 km^2.

Discussion

Solar's mean power density in 2016 was 5.4 $W_e\ m^{-2}$. Our approach for estimating the area of solar farms is not fully bottom-up so this estimate is subject to systematic error. It is possible, for example, that capacity densities have changed significantly given that the data used in our analysis is about 5 years old. That said, the assumption by (Jacobson *et al* 2018) that urban rooftops can be retrofitted with a capacity density 4.5-times higher than the commercial-scale solar plants measured by (Ong *et al* 2013) seems highly unlikely, as does the resulting 24–27 $W_e\ m^{-2}$ power density (Jacobson *et al* 2018). It is also possible that capacity densities vary strongly with larger size installations (see figure 2(A)). However, given that our analysis finds only a very weak relationship between module efficiency or installation size and capacity density, we expect the errors are small, likely less than 20%.

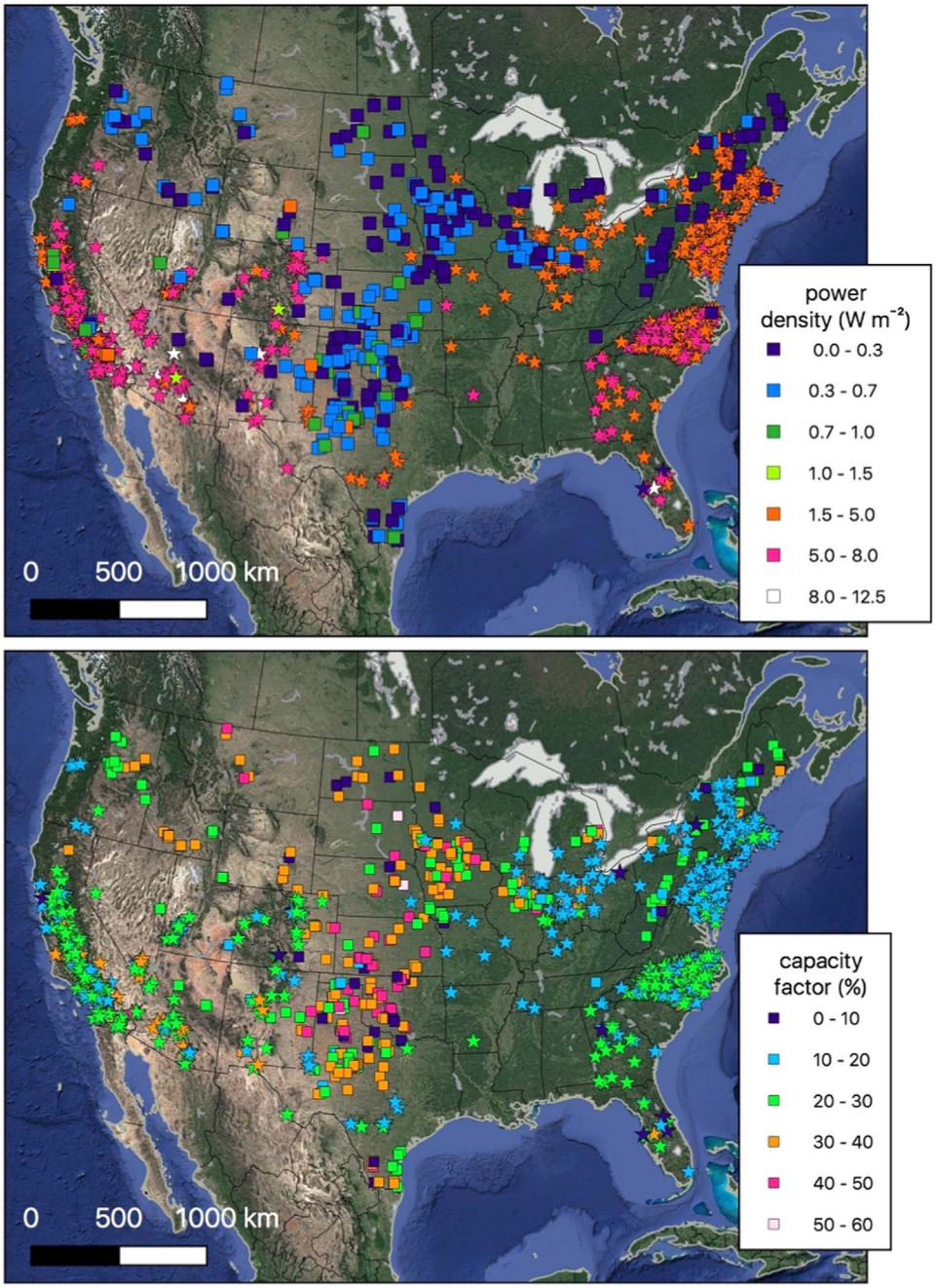

Figure 6. Spatial distribution of power density (top) and capacity factor (bottom) for 2016. Wind power plants represented as squares and solar power plants as stars.

Theoretically it is possible to attain high power densities with solar (120 W_e m^{-2} in Kammen and Sunter 2016) over small areas like an individual rooftop, but within the limitations of our data and analysis, we see no obvious trend towards increased solar power densities. Suggestions that solar power densities could be high enough to enable self-powered urban landscapes (Kammen and Sunter 2016) therefore seem implausible given the primary energy demand of large cities, such as Phoenix with a primary energy demand of 8.1 W m^{-2}, Los Angeles with 21 W m^{-2} or New York City with 69 W m^{-2}.

Wind's mean power density in 2016 was 0.50 W_e m^{-2}. This observed mean is consistent with estimates based on atmospheric theory and modeling (Gustavson 1979, Keith *et al* 2004, Wang and Prinn 2010, Miller *et al* 2011, Gans *et al* 2012, Jacobson and Archer 2012, Marvel *et al* 2012, Adams and Keith 2013, Miller *et al* 2015, Miller and Kleidon 2016) which predicted that large-scale wind power densities would be under 1.0 W_e m^{-2} and also that power densities will decrease with increasing size of the wind farm installation. This observed mean power density is much smaller than many common estimates (Archer and Jacobson 2005, Lu *et al* 2009, Sta. Maria and Jacobson 2009, Jacobson and Delucchi 2011, Lopez *et al* 2012, US Department of Energy 2015, World Bank Group and Technical University of

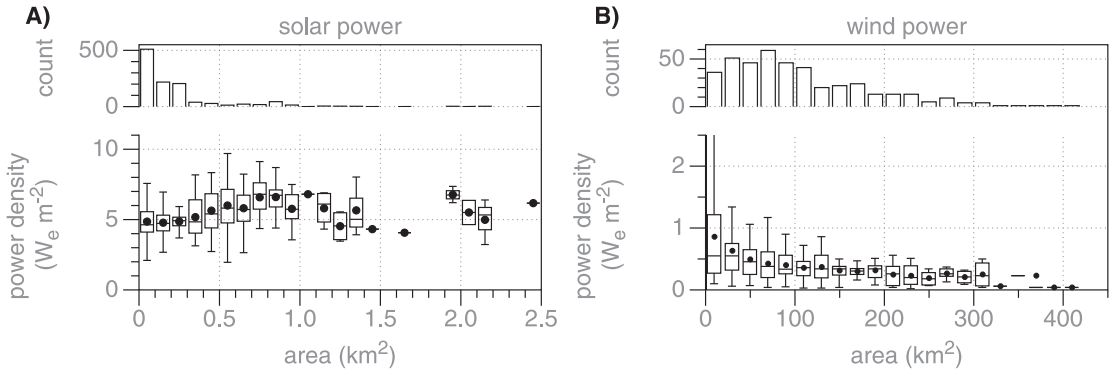

Figure 7. Power densities during 2016, binned by the area of the (A) solar power plant, or (B) wind power plant. Whisker plots show the interquartile range (IQR), with black points showing the mean of each area bin. Note that the solar areas are about 100-times smaller than the wind power plant areas.

Denmark 2018). Examples include 227 W m^{-2} over the windiest 10% of global land (World Bank Group and Technical University of Denmark 2018), 3.3 W_e m^{-2} over the entire Earth's surface (Jacobson and Delucchi 2011), 1.7 W_e m^{-2} over about 1/3 of the Continental US (Lopez *et al* 2012), or 1.4 W_e m^{-2} over about 2% of the US with excellent wind resources (US Department of Energy 2015). These are also by no means the highest estimates in the literature. For example, (World Bank Group and Technical University of Denmark 2018) quantify a wind power density of 808 W m^{-2} over the windiest 10% of US land, and (Kammen and Sunter 2016) estimated an upper bound of 35 W_e m^{-2} for wind power at urban-scales based on a study observing numerous vertical axis turbines which generated up to 47 W_e m^{-2} over an area of about 50 m^2 (Dabiri 2011).

There are two main reasons for these discrepancies in wind power density. First, many estimates did not account the interactions between wind turbine arrays and the atmospheric boundary layer. The limit to large-scale wind power density is the downward flux of kinetic energy from the free troposphere, a value that is about 1 W m^{-2} (Lorenz 1955, Peixoto and Oort 1992, Kim and Kim 2013). The effect of this atmospheric limit is illustrated by the relationship between wind power plant's area and power density. Second, many studies assume installed capacity densities which are too high. While we observed an average capacity density of 1.5 MW_i km^{-2}, (Rinne *et al* 2018) assume 5.5–9.4 MW_i km^{-2}, (Jacobson *et al* 2018) assume 7.2 MW_i km^{-2}, (Lopez *et al* 2012) assumed 5.0 MW_i km^{-2}, the US-DOE *Wind Vision: A New Era for Wind Power in the United States* (US Department of Energy 2015) assumed 3.0 MW_i km^{-2}. By assuming 2- to 6-times the observed capacity density but ignoring the atmospheric limits, these estimates resulted in power densities that are 2- to 6-times higher than observations.

Note that some important prior estimates from energy systems experts such as Ausubel (2007), MacKay (2013a) and Smil (2015) are much closer to our data-driven estimate.

Given that larger wind power plants have smaller power densities and given that a major increase in total wind power generation will presumably require expanding wind power plants into less-than-ideal locations, it seems likely that wind power density will decrease with time. It therefore seems—contrary to many prior estimates—unlikely that the power densities of greater than 1 W_e m^{-2} will be realized over substantial areas, and likely that average power densities will fall below 0.5 W_e m^{-2}.

As an example of the implications of these results, consider Germany and its ambitious energy transformation policy (Energiewende). Germany's primary energy consumption rate is 1.28 W m^{-2} (BP 2018). If our US wind power density of 0.50 W_e m^{-2} was applicable to Germany, then devoting all German land to wind power would meet about 40% of Germany's total primary energy consumption, while if German wind power performs like the best 10% of US wind (0.80 W_e m^{-2}), then generation would be 62% of Germany's consumption. Finally, if Germany's goal was to generate the most wind power without economic constraints, very high capacity densities (e.g. 10 MW_i km^{-2}) could be deployed, reducing capacity factors but possibly raising the power density to 1.0 W_e m^{-2} and meeting 80% of consumption. Whereas for solar at 5.4 W_e m^{-2}, 24% of Germany's land area would need to be devoted to commercial-scale solar to meet total primary energy consumption.

Of course, no such single-technology scenario is plausible. A mix of energy sources and storage is essential to addressing temporal and seasonal variability. Note that the amount of primary energy required to supply the same amount of final energy will fall with electrification and battery storage-reducing requirements, but using electricity to make gas or other

synthetic fuels has the opposing tendency. Yet, we hope this example illustrates the relevance of power density when planning for deep decarbonization.

Power densities clearly carry implications for land use. Meeting present-day US electricity consumption, for example, would require 12% of the Continental US land area for wind at 0.5 $W_e\,m^{-2}$, or 1% for solar at 5.4 $W_e\,m^{-2}$. US electricity consumption is just 1/6 total primary energy consumption (BP 2018), so meeting total consumption would therefore require 72% and 6% respectively for US wind and solar. Of course, like the Germany example, no single energy source is likely to ever supply all electric power. These comparisons nevertheless provide a benchmark for understanding the implications of power densities for land use, while recognizing that solar and wind power also occupy the area within the power plant boundary differently. These observation-based results should be considered in light of the fact that (a) decarbonizing the energy system will require considerably more primary power than current electricity demand, (b) demand may continue to grow, and finally, (c) that many areas of the world have higher energy demand per unit area than does the Continental US.

ORCID iDs

Lee M Miller https://orcid.org/0000-0001-5527-3194

References

Adams A S and Keith D W 2013 Are global wind power resource estimates overstated? *Environ. Res. Lett.* **8** 015021

Archer C L and Jacobson M Z 2005 Evaluation of global wind power *J. Geophys. Res.* **110** 1–20

Ausubel J H 2007 Renewable and nuclear heresies *Int. J. of Nuclear Governance, Economy and Ecology* **1** 229–43

BP 2018 BP Statistical Review of World Energy 2018 https://bp.com/content/dam/bp/en/corporate/pdf/energy-economics/statistical-review/bp-stats-review-2018-full-report.pdf (Accessed: 29 August 2018)

Dabiri J O 2011 Potential order-of-magnitude enhancement of wind farm power density via counter-rotating vertical-axis wind turbine arrays *J. Renew. Sustain. Energy* **3** 1–12

Denholm P, Hand M, Jackson M and Ong S 2009 Land-Use Requirements of Modern Wind Power Plants in the United States Land-Use Requirements of Modern Wind Power Plants in the United States *National Renewable Energy Laboratory* NREL/TP-6A2-45834 https://nrel.gov/docs/fy09osti/45834.pdf) (Accessed: 20 June 2018)

Gans F, Miller L M and Kleidon A 2012 The problem of the second wind turbine—a note on a common but flawed wind power estimation method *Earth Syst. Dyn.* **3** 79–86

Gustavson M R 1979 Limits to wind power utilization *Science* **204** 13–7

Hernandez R R, Hoffacker M K and Field C B 2014 Land-use efficiency of big solar *Environ. Sci. Technol.* **48** 1315–23

Hernandez R R, Hoffacker M K and Field C B 2015 Efficient use of land to meet sustainable energy needs *Nat. Clim. Change* **5** 353–8

Hoen B D, Diffendorfer J E, Rand J T, Kramer L A, Garrity C P and Hunt H E 2018 United States Wind Turbine Database. US Geological Survey, American Wind Energy Assocaition, and Lawrence Berkeley National Laboratory data release: USWTDB V1.0 (April 19, 2018). https://eerscmap.usgs.gov/uswtdb (Accessed: 20 June 2018)

Jacobson M Z and Archer C L 2012 Saturation wind power potential and its implications for wind energy *Proc. Natl Acad. Sci.* **109** 15679–84

Jacobson M Z and Delucchi M A 2011 Providing all global energy with wind, water, and solar power: I. Technologies, energy resources, quantities and areas of infrastructure, and materials *Energy Policy* **39** 1154–69

Jacobson M Z *et al* 2018 *Sustain. Cities Soc.* **42** 22–37

Kammen D M and Sunter D A 2016 City-integrated renewable energy for urban sustainability *Science* **352** 922–8

Keith D W, Decarolis J F, Denkenberger D C, Lenschow D H, Malyshev S L, Pacala S and Rasch P J 2004 The influence of large-scale wind power on global climate *Proc. Natl Acad. Sci.* **101** 16115–20

Kim Y-H and Kim M-K 2013 Examination of the global Lorenz energy cycle using MERRA and NCEP-reanalysis 2 *Clim. Dyn.* **40** 1499–513

Lopez A, Roberts B, Heimiller D, Blair N and Porro G 2012 US Renewable Energy Technical Potentials : A GIS-Based Analysis *NREL/TP-6A20-51946* https://nrel.gov/docs/fy12osti/51946.pdf (Accessed: 20 June 2018)

Lorenz E N 1955 Available potential energy and the maintenance of the general circulation *Tellus* **7** 157–67

Lu X, McElroy M B and Kiviluoma J 2009 Global potential for wind-generated electricity *Proc. Natl Acad. Sci.* **106** 10933–8

MacKay D J C 2009 *Sustainable Energy—Without the Hot Air* (Cambridge, UK: UIT Cambridge Ltd)

MacKay D J C 2013a Could energy-intensive industries be powered by carbon-free electricity? *Phil. Trans. R. Soc. A* **371** 20110560

MacKay D J C 2013b Solar energy in the context of energy use, energy transportation and energy storage *Phil. Trans. R. Soc. A* **371** 20110431

Marvel K, Kravitz B and Caldeira K 2012 Geophysical limits to global wind power *Nat. Clim. Change* **2** 1–4

Miller L M, Brunsell N A, Mechem D B, Gans F, Monaghan A J, Vautard R, Keith D W and Kleidon A 2015 Two methods for estimating limits to large-scale wind power generation *Proc. Natl Acad. Sci.* **112** 11169–74

Miller L M, Gans F and Kleidon A 2011 Estimating maximum global land surface wind power extractability and associated climatic consequences *Earth Syst. Dyn.* **2** 1–12

Miller L M and Kleidon A 2016 Wind speed reductions by large-scale wind turbine deployments lower turbine efficiencies and set low generation limits *Proc. Natl Acad. Sci.* **113** 13570–5

Ong S, Campbell C, Denholm P, Margolis R and Heath G 2013 Land-Use Requirements for Solar Power Plants in the United States *NREL/TP-6A20-56290* https://nrel.gov/docs/fy13osti/56290.pdf (Accessed: 20 June 2018)

Peixoto J P and Oort A H 1992 *Physics of Climate* (New York: Springer-Verlag)

QGIS Development Team 2018 QGIS geographic information system Open Source Geospatial Foundation Project https://www.qgis.org/en/site/

Rinne E, Holttinen H, Kiviluoma J and Rissanen S 2018 Effects of turbine technology and land use on wind power resource potential *Nat. Energy* **3** 494–500

Smil V 1984 On energy and land *Am. Sci.* **72** 15–21

Smil V 2015 *Power Density: A Key to Understanding Energy Sources and Uses* (Cambridge, MA: MIT Press)

Sta. Maria M R V and Jacobson M Z 2009 Investigating the effect of large wind farms on energy in the atmosphere *Energies* **2** 816–38

US Department of Energy 2015 Wind Vision: a new era for wind power in the United States https://www.nrel.gov/docs/fy15osti/63197-2.pdf (Accessed: 1 Oct 2018)

US Energy Information Administration (EIA) 2018a Power Plants Shapefile https://eia.gov/maps/map_data/PowerPlants_US_EIA.zip (Accessed: 1 Oct 2018)
US Energy Information Administration (EIA) 2018b Bulk Electricity Data https://eia.gov/opendata/ (Accessed: 20 June 2018)
US Energy Information Administration (EIA) 2018c Form EIA-860 Detailed Data https://eia.gov/electricity/data/eia860/ (Accessed: 20 June 2018)
US Energy Information Administration (EIA) 2018d Electric Power Monthly with Data for March 2018 https://eia.gov/electricity/monthly/current_month/epm.pdf (Accessed: 20 June 2018)
Wang C and Prinn R 2010 Potential climatic impacts and reliability of very large-scale wind farms *Atmos. Chem. Phys.* **10** 2053–61
World Bank Group and Technical University of Denmark 2018 Global wind atlas https://globalwindatlas.info/ (Accessed: 5 September 2018)